Mechanistic Investigation of Char Growth from Lignin Monomers during Biomass Utilisation

Alexander Shaw[1,3], Xiaolei Zhang[1*], Shuya Jia[1], Juan Fu[2], Lin Lang[2,5*], Robert C Brown[4]

[1] Department of Chemical and Process Engineering, University of Strathclyde, UK

2 CAS Key Laboratory of Renewable Energy, Guangzhou Institute of Energy Conversion, Chinese Academy of Sciences (CAS), China.

[3] Department of Chemical & Biological Engineering, Northwestern University, USA

[4] Department of Mechanical Engineering, Iowa State University, USA

[5] Guangdong Key Laboratory of New and Renewable Energy Research and Development, China.

ABSTRACT

Char is formed as a significant product from the pyrolysis of biomass, and it is well reported that lignin is the greatest contributor to the production of char. The structures of lignin chars are well studied in literature; however, an elucidation on the lignin char formation mechanism is lacking and this is essential to achieve precise control of biomass thermal conversion. In this work, the char growth process from β-O-4 linkage derived lignin monomers was investigated using density functional theory (DFT) and validated by slow pyrolysis experiments and Nuclear Magnetic Resonance (NMR) analysis. It was shown that char forms in a two-step process, beginning with the aggregation of two mono-aromatic species to yield tricyclic species, which then participate in further ring forming reactions to yield larger aromatic clusters. The side products generated involve hydrogen, water, methanol, and formaldehyde. Insights from the proposed mechanism are important for guiding future research on char formation during biomass thermochemical conversion processes.

1. Introduction

It is globally imperative to produce energy and materials from renewable sources aiming to reduce reliance on fossil fuels, curtail CO_2 emissions, and achieve net zero targets. Biomass, including wood, grasses and agricultural waste, are widely available renewable sources of both energy and industrially important chemical precursors. It is commonly known that energy potential of biomass (heat and electricity) can be exploited via combustion; while fuels and chemical products can be obtained by biomass thermal deconstruction through pyrolysis or gasification [1–3]. The thermal deconstruction of biomass can be described as biomass feedstock firstly being converted into primary decomposition products (bio-oil, syngas, and char), which will further be upgraded into fuels and chemicals. Amongst all three types of biomass primary decomposition products, char takes up large quantities, often accounting for 30-40wt% [4–6]. An inconsistent definition of the characteristics of pyrolysis chars has led some literature sources to report char yields as high as 90% at lower pyrolysis temperatures, though this will certainly include significant proportions of unreacted and partially reacted feedstock materials. The inclusion of large quantities of unreacted biomass within reported char yields hampers efforts at understanding the mechanisms by which char forms, particularly given that the structure of the remaining solids are known to be highly dependent on temperature.

The structure of bio-chars varies with different operating conditions (e.g. temperature, heating rate)[7] and technology (e.g. slow pyrolysis, fast pyrolysis, gasification) [8–10]. It has been shown that increasing pyrolysis temperatures causes a large reduction in the concentration of aliphatic, hydroxy, and methoxy functionalities in chars. Additionally, identification of increasing aromatic ^{13}C nuclear magnetic resonance (NMR) signals alongside aromatic CH infrared stretches provides strong evidence for the development of a highly aromatic char structure under higher pyrolysis temperatures. An in-depth analysis of chars formed under three different pyrolysis conditions by Brewer et al. [4] revealed that all chars possessed a condensed aromatic structure with some oxygen containing edge functionalities. It was shown through quantitative ^{13}C NMR analysis that the size of char clusters formed during slow and fast pyrolysis were similar in size, while those formed from gasification were larger [4].

Within the three biomass components (cellulose, hemicellulose, and lignin), it was found that the greatest quantities of biochar are formed from pyrolysis of lignin [11] [12]. A direct correlation between biomass lignin content and the yield of char formed was reported by Demirbas [13] at

temperatures of 650 °C and above. This is in agreement with other studies that showed a higher incidence of char formation during the pyrolysis of lignin over polysaccharides [14,15]. As the most common linkage that is found in lignin contains a β-O-4 ether bonds,[16] it is common practice to use β-O-4 containing model compounds for lignin, for example, phenethyl phenyl ether (PPE) and its derivatives [17,18].

Drage et al. [19], conducted slow pyrolysis experiments of two model compounds containing β-O-4 bonds in a closed system at 300 °C. All of the products identified were phenolic, suggested they were formed from the ether oxygen bearing ring following cleavage of the ether C-O bond. As none of the aliphatic ring bearing products were identified, it was proposed that they were consumed during formation of the large amounts of char. To test this hypothesis, the slow pyrolysis char was collected and then subjected to fast pyrolysis. The products obtained from this additional pyrolysis step had characteristics which indicated that they had been formed from the missing aliphatic bearing portion of the original model compounds, thus evidencing that the aliphatic bearing portion had been consumed during char formation.

Some studies, including experimental work from Britt et al. [20] as well as theoretical work from Huang et al. [21,22], have proposed that the β-O-4 linkages decompose through homolytic cleavage pathways. Other works, like those of Jarvis et al. [17], Klein and Virk [23] and Huang et al. [21] have shown that a more facile route for β-O-4 cleavage is via one of two concerted mechanisms. These are a 4-centred Maccoll elimination and a 6-centred retro-ene fragmentation, which when applied to unsubstituted PPE will yield phenol and styrene. Later works showed that substitution of the α and β carbons, and inclusion of aromatic methoxy groups on the rings, gives rise to more complex propenyl benzene derived species [18,24–26].

Despite ample evidence as to the origin of lignin pyrolysis char, no clear formation mechanisms have yet been put forward. Drawing upon previous experimental observations within the literature, in this work we identify and explore the first mechanisms for the formation of lignin char. Employing density functional theory calculations, we first analyse 16 potential pathways for the concatenation of two β-O-4 decomposition products. The product of all 16 pathways is a 3 ringed polycyclic aromatic species that can engage in further ring forming reactions to yield aromatic clusters of similar structure to those reported by Brewer et al. [4]. One example pathway of this ring growth process is also explored using density functional theory (DFT). Slow pyrolysis of

the structurally analogous cinnamyl alcohol followed by NMR analysis were carried out to validate the modelling results.

Clearer understanding of the mechanisms by which char forms from lignin will afford greater influence over the characteristics and yields of carbonaceous materials synthesised from lignin. Furthermore, it is hoped that the underlying mechanisms proposed herein can be used to guide studies on formation of chars from other biomass sources.

2. Methodology

2.1. Computational details

All calculations were performed using the M052X [27] functional, which has been employed previously to investigate the thermal conversion reactions of biomass [28–31]. A thorough assessment of an array of DFT methods by Goerigk, Grimme and co-workers [32] showed that M052X performed second best in class among the hybrid methods, with only ωB97X-V [33] outscoring it in terms of its weighted mean deviation score. M052X also performed well when assessed for accuracy in calculating reaction barrier heights across a range of pericyclic reactions, with a root mean squared deviation of just 1.7 kcal mol^{-1} [34]. The general broad purpose accuracy of the M052X functional[35,36], and its specific utility for calculation of pericyclic reactions, makes it an ideal choice of method for the present study. Dispersive effects are accounted for by inclusion of Grimmes D3 empirical dispersion correction [37,38], though zero damping function is used due to incompatibility with the Minnesota family of functionals.

To further ascertain appropriateness of the chosen functional, we calculated the energy barrier for the intermolecular Diels-Alder reaction of styrene at both the M052X level and the high accuracy G3B3 [39] composite method. The barrier height for the Diels-Alder cycloaddition of styrene was calculated as 28.2 kcal mol^{-1} at the G3B3 level and was found to be 27.9 kcal mol^{-1} at the M052X-D3/Def2-TZVP [40] level. This minor difference of 0.3 kcal mol^{-1} further supports our choice of functional for this study. Assessment of the choice of basis set is provided in the supplementary information.

All ground state structures were confirmed as having zero imaginary frequencies, while transition state structures were confirmed to have just one imaginary frequency. Intrinsic reaction coordinate calculations were used to link transition states to reactants and products. All calculations assume standard temperature and pressure (298.15 K and 1 atm) and the default integration grid of 99,590 was used in all calculations. Gaussian 16 Rev. A [41] was used to perform all calculations.

2.2. Experimental set up

A lab-scale fixed-bed stainless steel reactor (as shown in Figure 1), which was reported in our previous paper [42], was used to investigate the pyrolysis characteristics of the cinnamyl alcohol (CnA, 97.5%), one model compound of propenyl benzene derivatives, in the pure N_2 gas (99.99%) at 300 °C [43]. Firstly, about 3.0 g of CnA was sealed in the stainless-steel reactor that has internal and external diameters of 30 mm and 60 mm, respectively. Secondly, the CnA sample was swept by pure N_2 gas with a flow of 100 mL/min for about 1.0 hour to exhaust the air, then the CnA was sealed in dry nitrogen at room temperature. Thirdly, the stainless-steel reactor was installed vertically in the electric furnace and heated to 300 ºC, the reaction was then carried out at 300 ºC for 20 hours and 100 hours, respectively. Finally, the hot reactor was quickly taken out, and naturally cooled down at room temperature.
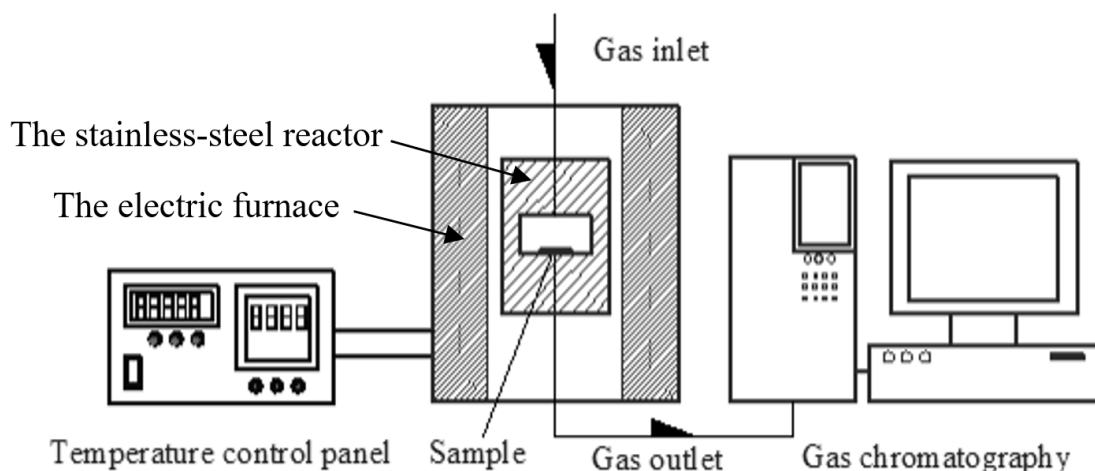

Figure 1. The experimental configuration of the fixed-bed stainless steel reactor [42].

^{13}C NMR experiments were performed using a solid-state NMR spectrometer (AVANCE Ⅲ WIDE BORE 300, Bruker, Germany) operating at 75 MHz using a 4 mm probe. Quantitative ^{13}C Direct Polarization/Magic Angle Spinning (DP/MAS) NMR experiments were performed by high power proton decoupling method (HPdec), using 4-mm sample rotors at a spinning frequency of 6500 Hz. The ^{13}C 90°-pulse length was 4.5 μs, and pulse length in decoupling sequence is 5.40. The carbon resonance line of adamantane was used as an external chemical shift standard and was assigned a value of 38.48 ppm. The scans for HPdec experiments were 10000. To prepare the solid samples, the CnA and chars were mixed with the SiO_2 powders (99.9%) for NMR tests.

3. Results and Discussion

We have observed that char growth from the β-O-4 containing model compounds can be described as a two-step process, beginning with an initiation step that concatenates two single-ring aromatic compounds to form a three-ring species, and a further cluster aggregation process that expands the char cluster by addition of further mono-aromatic species.

3.1. Initiation: one-ring to three-ring structure

3.1.1 Stereoisomers and 16 pathways

The oxygenated propenyl benzene derivative is the selected model compound of lignin for the modelling work. Owing to the presence of both *erythro-* and *threo-* forms of the β-O-4 linkage in native lignin[44,45], both the cis and trans isomers (shown in Figure 2a) will be formed from the β-O-4 linkage breaking, so we have chosen to include both isomers in this study. The initiation step concatenates two β-O-4 derived model compounds into one complex which, due to the cis and trans isomerism, gives rise to four possible diene-dienophile pairings: cis-cis (CC), cis-trans (CT), trans-cis (TC), and trans-trans (TT), where the first letter indicates the isomerism of the diene, and the second letter indicates the dienophile. The two elimination reactions that follow the cycloaddition reaction are also dictated by the isomerism of the reaction species owing to the accessibility of the leaving groups to participate in the reactions. This means that each diene/dienophile pairing follows a unique reaction pathway consisting of three elementary reactions.
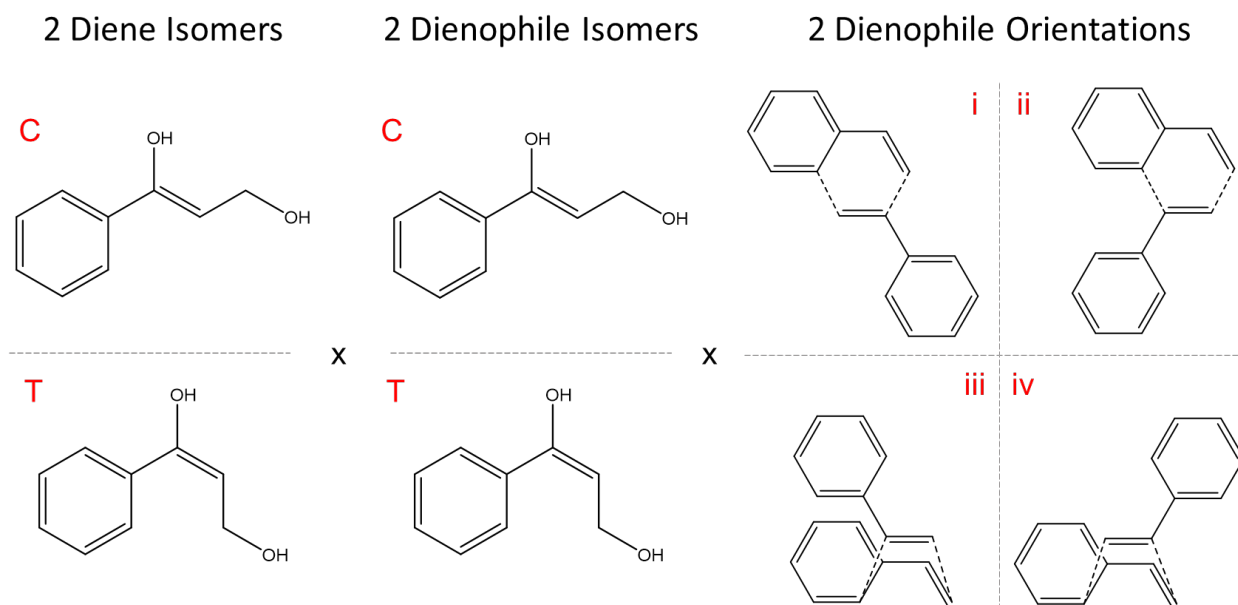
Figure 2. The two possible isomers for both the diene and the dienophile that give rise to the four isomer pairs. These pairings are labelled as CC, CT, TC, and TT, where the isomer of the diene is given by the first letter and the dienophile by the second. The four orientations of the dienophile that can participate in the Diels-Alder reaction are also provided in Figure 2. These orientations, denoted as i-iv, are obtained through 180° rotation of the dienophile about any principal axis and can be understood analogously to the symmetry operations of ethylene.

In this work we have considered four possible orientations for the cycloaddition reaction. These four orientations are shown in Figure 2. Combining the four possible pairings of reactants (CC, CT, TC, and TT) and the four possible approaches, gives rise to 16 pathways in total. We have denoted each of the four orientations with the letters i-iv, as shown in Figure 2.

3.1.2 Diels-Alder cycloaddition and Elimination reactions

For the char growth from one-ring to three-ring, the first elementary reaction consists of a Diels-Alder cycloaddition between two molecules of the model compound, where one acts as a diene and the other as a dienophile. Various types of elimination reactions (dehydrogenation, dehydroxymethanation, dehydration, or grob fragmentation) will be followed to release the minor compounds (H_2, methanol, water, or formaldehyde) and form a three-ring char structure (Prod-3ring). The optimal reactions for the initiation step are shown in Figure 3.

Following the Diels-Alder cycloaddition, there are two potential elimination reactions that occur as the second elementary reaction based upon the isomerism of the diene. When the diene is in the form of the cis isomer, as with is the case for the CC and CT pairs, a cross-ring dehydrogenation reaction is favoured (from Inte1 to Inte2 for CC and CT). Due to the orientation of the hydroxymethyl group, it is difficult for the two trans diene complexes, TC and TT, to undergo a dehydrogenation reaction. Alternatively, elimination of methanol via dehydroxymethanation is possible through a 6-membered pericyclic transition state (from Inte1 to Inte2 for TC and TT). The final mechanism in all pathways of sets CC and TC is a double elimination reaction, a form of Grob fragmentation, that produces water and formaldehyde (from Inte2 to Prod-3ring for CC and TC). There is no Grob fragmentation transition state obtained for sets CT and TT, owing to non-coplanarity of the hydroxy and the hydroxymethyl group. An alternative reaction is a 4-centred elimination to yield water via dehydration (from Inte2 to Prod-3ring for CT and TT).

The activation barriers and reaction energies for those reactions are shown in Figure 4. From the energy changes from reactant to products, it can be seen that all the 16 pathways are exothermic with the TT pairs release the highest energy and the CC pairs release the lowest energy. Regarding the energy barriers, the Diels-Alder cycloaddition has the lowest energy barrier (ranges 27.8-37.2 kcal/mol), the two elimination steps have the similar range of activation energy, which are the rate-limiting steps. We observe that the CC pathways generally have the lowest activation energies but are also the least enthalpy releasing. In contrast to this we find that the TT pathways have the highest activation energies and are also the most enthalpy releasing. All the reactions are spontaneous due to the negative Gibbs free energy change at each step.
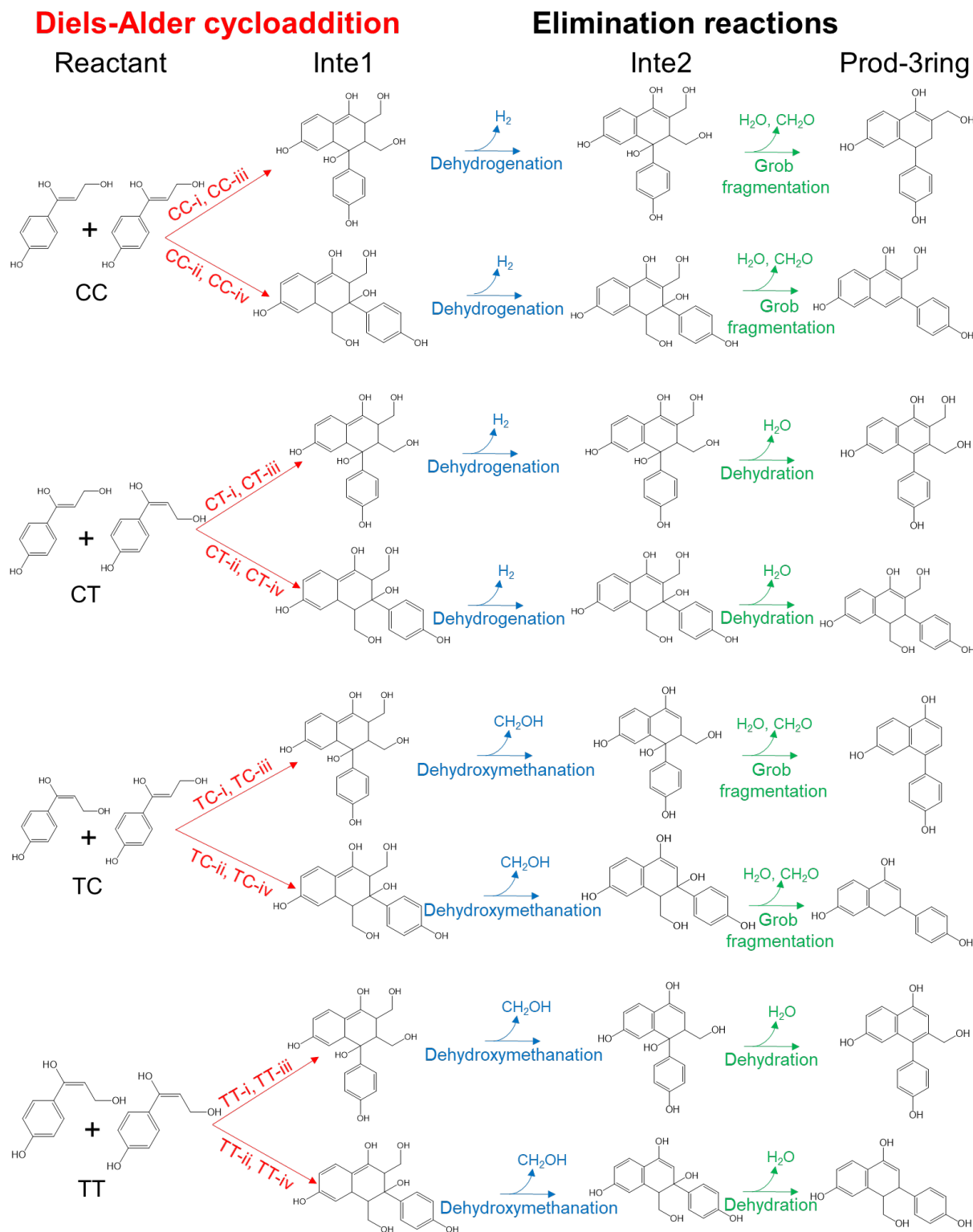
Figure 3. Various Diels-Alder cycloaddition and elimination reactions involved in the initiation step, all 16 pathways were considered. Pathways labelled i and iii, and ii and iv are presented together owing to the formation of identical prod-3ring structures.
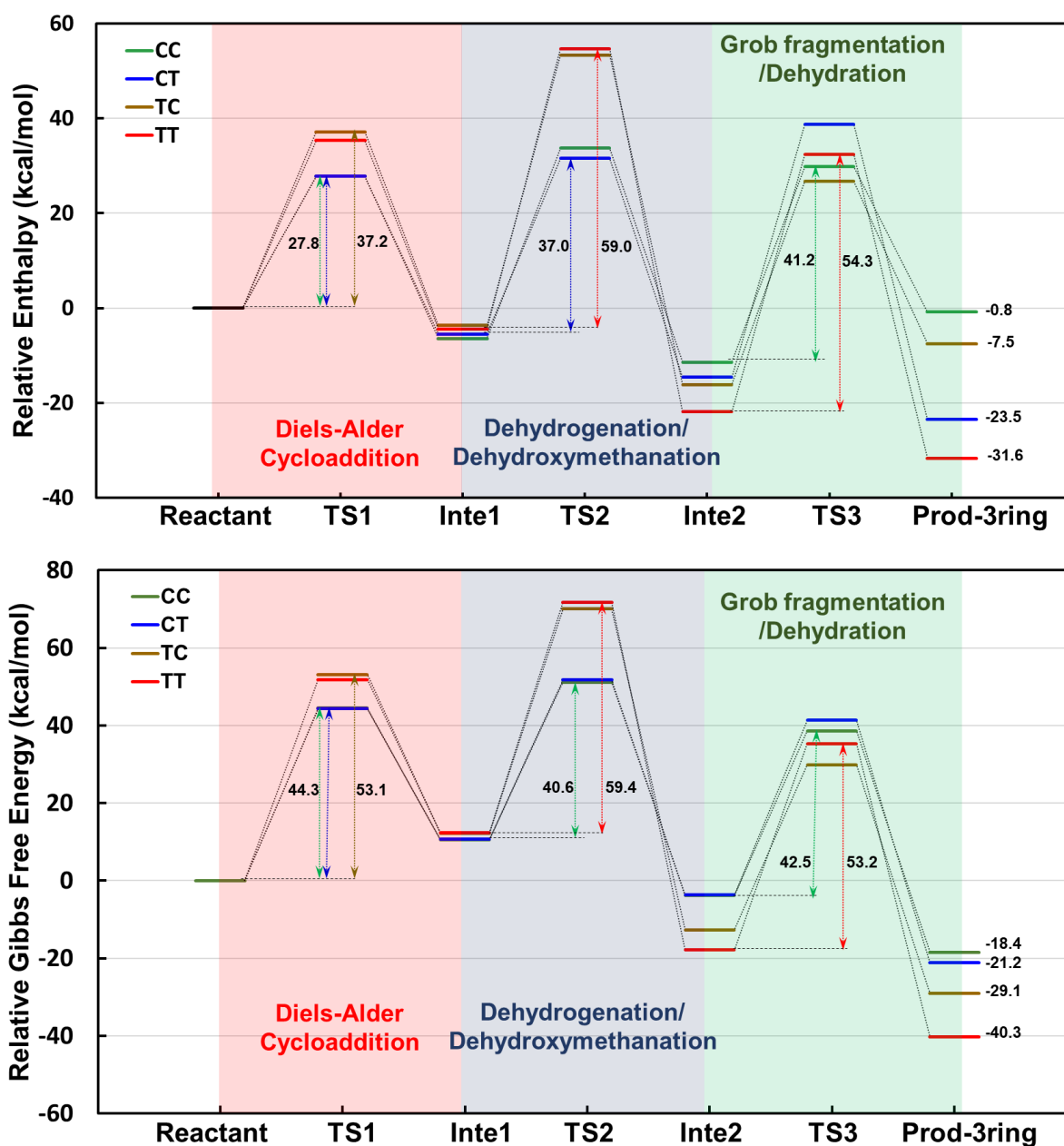
Figure 4. Enthalpy changes and Gibbs free energy changes of the reactions involved in the initial steps. For each pairing of the reactants (CC, CT, TC, TT), the energies here shows the average value of the four possible orientations, for example, CC value here shows the average of the CC-i, CC-ii, CC-iii, CC-iv. TS1, TS2, TS3 represent three transition states; Inte1 and Inte2 represent two intermediates; Prod-3ring represent the 3-ring product from the initial step. The detailed

structure of all the compounds (transition states, intermediates, and products) can be found in Figure 3.

For the Diels-Alder cycloaddition, the CC and CT pathways exhibit lower energy barriers that the TC and TT pathways. Despite this variety found for the Diels-Alder cycloaddition values, they do correlate well with other computational findings. Khuong et al. [46] calculated the energy barriers for the proposed cycloaddition dimerisation of styrene [47], reporting activation energies of between 27.7 kcal mol^{-1} and 35.6 kcal mol^{-1}, in good agreement with the upper and lower bounds of the cycloaddition barrier heights in the present work. Variation between the literature study and the present results is expected given the various oxygen functional groups of the reactants in this work and the different choice of computational methodologies.

In general, the barrier heights for the cross-ring dehydrogenation in the CT pathways are more favourable than for the CC pathways. In both groups, the dehydrogenation is reasonably exothermic and more notably exergonic. Experimental reports of the activation barrier for the comparative dehydrogenation of 1,4-cyclohexadiene provide values of 42.7 kcal mol^{-1} [48] to 43.8 kcal mol^{-1} [49]. These experimental values are close to the maximum barrier heights of the analogous dehydrogenation reactions in the present work, which are likely facilitated by the shorter inter-hydrogen distances in all Inte1 complexes when compared to the planar geometry of 1,4-cyclohexadiene [50]. In competition with the dehydrogenation step is a retro-Diels-Alder reaction to reform the two starting species [51,52]. With a lower activation energy and higher reaction enthalpy, this reverse reaction is the kinetically controlled route while the dehydrogenation is the thermodynamically controlled pathway.

There is a distinct paucity of reports regarding dehydroxymethylation reactions within the literature[53–55], and those that were identified are concerned with catalytic processes., This makes direct comparison of calculated reaction barrier heights and enthalpies to empirical values difficult. The dehydroxymethylation reactions that we have proposed here appear to be the first reported concerted mechanisms for methanol formation during lignin pyrolysis. Allan and Matilla [56] proposed that methanol is derived from aromatic methoxy groups from the lignin; however, this requires high energy due to the homolytic cleavage of such groups. Klein and Virk [57] suggested that methanol is derived from cinnamyl alcohol functional groups in lignin, yet pyrolysis studies of cinnamyl alcohol [58], p-coumaryl alcohol [59], and other lignin model compounds that have such functional groups [60] have not reported the formation of methanol.

The Grob fragmentation in all pathways is reasonably endothermic (from Inte2 to Prod-3ring for CC and TC). This reaction has been proposed to occur in the pyrolysis of glycerol in two earlier works [61,62]. High level quantum chemical calculations by Nimlos et al. [61] give an energy barrier for this fragmentation of 65.2 kcal mol^{-1}, starkly contrasting the lower barriers of 41.2 kcal mol^{-1} calculated in this work. The Grob fragmentations in the present study are less endothermic than that of glycerol, which is likely the result of the aromaticity that is generated in the newly formed ring, as well as the planarity of all bonds within the ring system. At present, formaldehyde formation from lignin is mainly understood to be a result of the thermal scission of hydroxyl bearing aliphatic groups, however, if the formation is to proceed via homolytic pathways, significant energy requirements must be overcome. For example, Khachatryan et al. [58] calculated the bond dissociation enthalpy for cleavage of a hydroxymethyl group from cinnamyl alcohol to be 90.7 kcal mol^{-1}. The significantly lower activation energies of the Grob fragmentation in this work provide a potentially more facile route for the formaldehyde formation from lignin and agree with the literature reports in which formaldehyde is observed to form at lower pyrolysis temperatures [63].

The activation energies for the dehydration reaction in the final step are notably larger than those observed for any of the Grob fragmentation reactions, averaging 54.3 kcal mol^{-1} for TT. Conversely to the Grob fragmentation reactions, all dehydration pathways are exothermic and correspondingly all are over 19.0 kcal mol^{-1} free energy releasing. The analogous literature reaction is the dehydration of ethanol, which was studied by Sivaramakrishnan and co-workers [64] using high level quantum chemical calculations. This simpler reaction was found to have a higher energy barrier of 66.0 kcal mol^{-1}, compared to 49.6 to 57.2 kcal mol^{-1} for the dehydrations in the present work. The reduced enthalpy of reaction of the dehydrogenations proposed in this work compared to the literature example mimics the pattern observed for the Grob fragmentations and we can again attribute this to the induction of resonance in the newly formed compound.

3.2. Cluster Aggregation: three-ring to five-ring structure

Patently, the phenyl-naphthalene derivatives form from the initiation step are not structurally representative of the lignin-derived aromatic clusters. To form the larger polycyclic structures, further Diels-Alder cycloadditions occur owing to the ability of the intermediate compound to act once more as a diene. This is followed by intramolecular eliminations of the type already

described. The newly formed product can continue this pattern of ring-formation and eliminations to grow the aromatic structure further. A generalised scheme for these cluster aggregation reactions is provided in Figure 5. The shape of the growing clusters will depend upon the orientation of the joining dienophile as this will control the orientation of the diene, and therefore placement of the new ring structure, on the newly formed char. Furthermore, it can be seen that the isomerism of the dienophile will again affect the nature of the elimination reaction, as was the case for all initiation reactions, and will therefore also affect the oxygen functionality present upon the char.
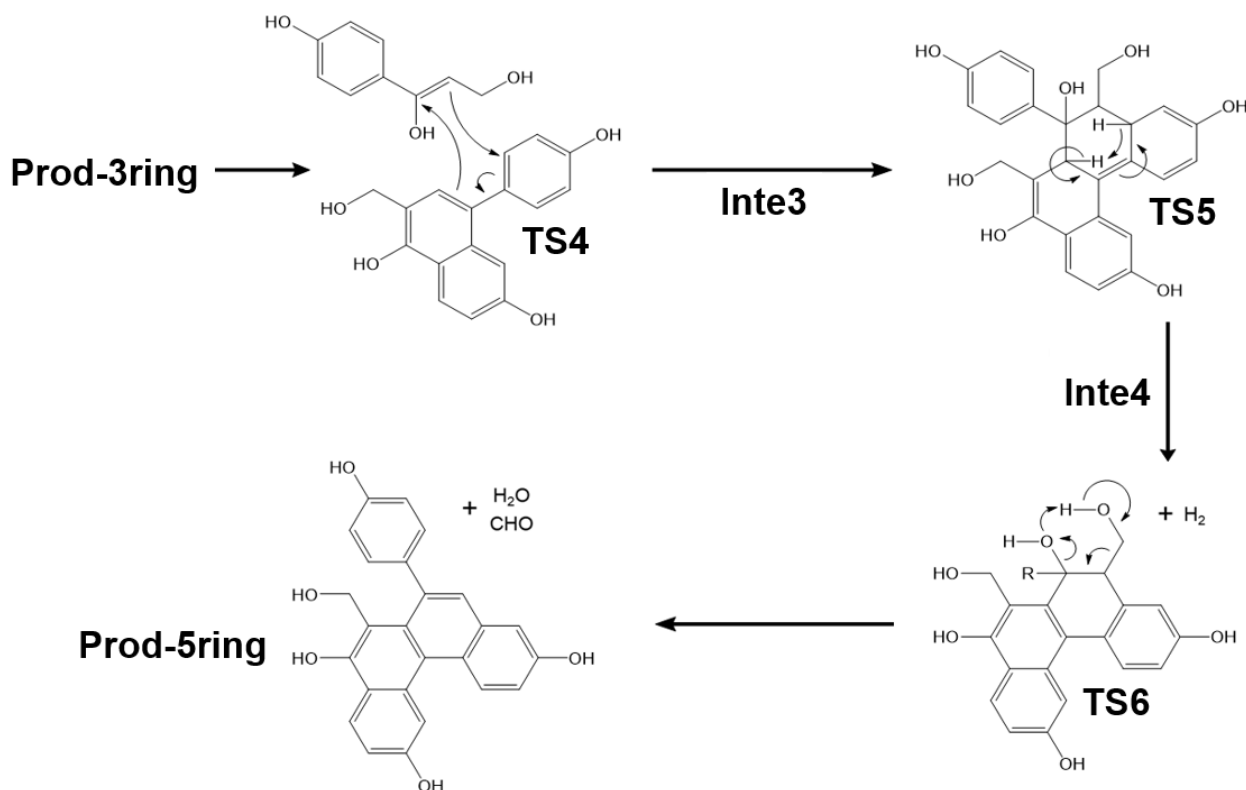

Figure 5. General scheme for the cluster aggregation reaction from 3-ring structure to 5-ring structure.

To explore the activation energies for aromatic cluster aggregation, the cluster aggregation pathway beginning with the reaction of a cis-dienophile with the CC-i-Product was modelled. Table 1 lists the obtained energies (enthalpies and free energies) of the elementary reactions.

Table 1. Activation barriers and reaction enthalpies (in kcal/mol) for each reaction of the aggregation step.

TS4		Inte3		TS5		Inte4		TS6		Prod-5ring	
ΔH	ΔG	ΔH	ΔG	ΔH	ΔG	ΔH	ΔG	ΔH	ΔG	ΔH	ΔG

| 40.8 | 58.1 | 16.6 | 34.3 | 36.6 | 36.9 | -29.6 | -38.0 | 55.5 | 54.7 | 22.5 | -2.8 |

The activation energy for the Diels-Alder reaction for cluster aggregation is higher than for any of the cycloaddition reactions presented so far at 40.8 kcal mol^{-1}. We also observe a relatively high energy of the cycloaddition product of 16.6 kcal mol^{-1}, which means that the cluster aggregation reaction contains the only notable endothermic Diels-Alder reaction. The first of the elimination reactions is cross-ring dehydrogenation of the type previously described in this work. The enthalpy barrier for this step is 36.6 kcal mol^{-1} which is similar to those observed for the CC and CT pathways. Interestingly, the dehydrogenation is notably more exothermic than is the case for the CC and CT pathways. The final step of this aggregation pathway is a Grob fragmentation which proceeds through a high energy barrier of 55.5 kcal mol^{-1}. The more endothermic cycloaddition reaction leads to a higher overall energy barrier for cluster aggregation than was observed for any of the 16 initiation pathways.

3.3. NMR Results

The HPdec spectrum from the NMR result are shown in Figure 6. The relative aromatic carbon fraction values (aromaticity), which contain the carbon atoms conjugating with phenyl ring, can be calculated from the quantitative ^{13}C NMR data [65]. In detail, the integral obtained from 115 to 150 ppm (mostly aromatic carbons) is recorded as A and the integral of the total NMR spectrum (e.g., from -10 to 225 ppm) is recorded as T. The relative aromaticity (f_a) can be calculated by the area ratios (f_a=A/T). The f_a value for the reactant CnA and the pyrolysis product chars are shown in Table 2. It can be seen that the aromaticity increased significantly from the feedstock CnA to its product char (from 76.99% to 89.13%).

Further analysis was carried out to find out the carbon numbers in the reactant and product compounds. Brewer et.al. [4] proposed that the degree of aromatic condensation can be estimated by the fraction of carbons along the edges of the aromatic rings, X_{edge}=1-X_{bridge}, which decreases with increasing aromatic ring cluster size. Usually, the aromatic edge carbons in chars come from aromatic C-H and aromatic C-O moieties, whose fractions X_{Ar-H} (f_{Ar-H}/f_{Ar}) and X_{Ar-O} (f_{Ar-O}/f_{Ar}) can be determined from the NMR spectra. (f_{Ar}, f_{Ar-H}, and f_{Ar-O} stand for aromatic carbon fractions: total aromatic carbon, aromatic carbon bonded to hydrogen, and aromatic carbon bonded to oxygen,

respectively.) Together, they constitute the minimum aromatic edge fraction ($X_{edge,min}$) as shown in Equation 1.

$$X_{edge,min} = X_{Ar-H} + X_{Ar-O}$$
Equation 1

Additional contributions can come from alkyls-C ($X_{Alkyls}=f_{Alkyls}/f_{Ar}$) and carbonyls-C ($X_{Carbonyls}=f_{Carbonyls}/f_{Ar}$) bonded to the aromatic rings. Thus, the upper limit of the edge fraction ($X_{edge,max}$) is provided by Equation 2.

$$X_{edge,max} = X_{edge,min} + X_{Alkyls} + X_{Carboxyls}$$
Equation 2

Considering the oxygen containing groups were not found in the pyrolysis chars, the formula (2) was simplified as $X_{edge,max} = X_{Ar-H} + X_{Alkyls}$, and one can calculate the minimum number of carbons ($n_{c,min}$) in a cluster relates to the edge fraction by Equation 3 [4,66].

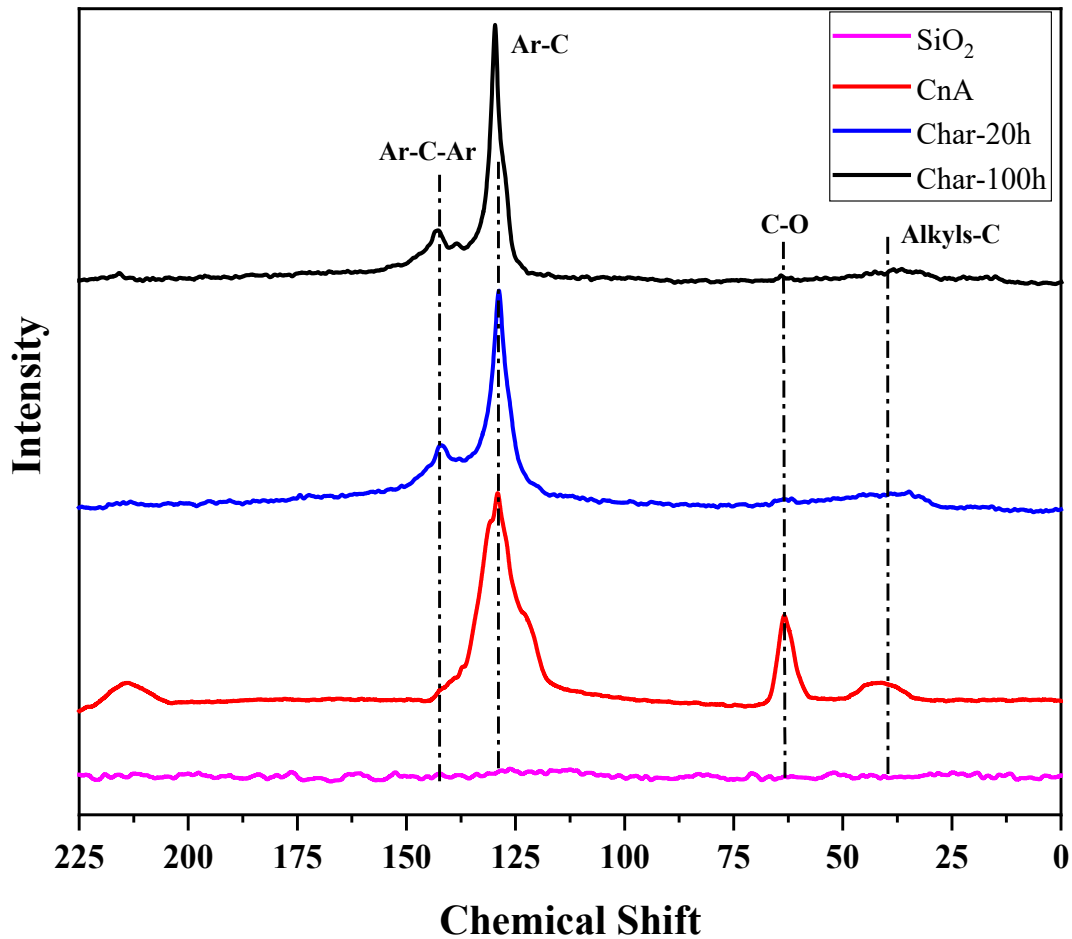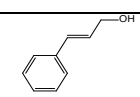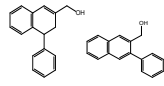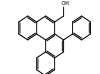$$n_{c,min} \geq 6/X_{edge}^2 \geq 6/X_{edge,max}^2$$
Equation 3

Figure 6. The NMR spectrum for the reactant CnA and the produced chars.

As shown in Table 2, the reactant has more than 6 carbons, and the char with a pyrolysis time of 20 hours has more than 12 carbons, and the char with pyrolysis time of 100 hours has more than 23 carbon numbers. It is clear that longer pyrolysis time shows higher aromatization. The overall trend fits well with the DFT calculations that the carbon numbers for the reactant, prod-3ring, and prod-5ring are **7**, 17, and 25, respectively. This validated again the aromaticity of the char formation process.

Table 2. Aromaticities and the carbon numbers for CnA and the produced char.

	NMR Results					DFT results		
Sample	Aromaticity	X_{Ar-H}	X_{Alkyls}	$X_{edge,max}$	$n_{C,min}$	Compound	Structure	n_C
CnA	76.99%	0.908	0.066	0.974	≥6	CnA		7
Char-20h	87.00%	0.571	0.125	0.696	≥12	Prod-3ring		17
Char-100h	89.13%	0.394	0.117	0.511	≥23	Prod-5ring		25

3.4. Char growth mechanism

Summarising the modelling and the NMR results, here we propose a two-stage mechanism that begins with an initiation stage that combines two mono-aromatic compounds to produce small aromatic species. The second stage is the subsequent growth of aromatic clusters by addition of further mono-aromatic compounds. A generalised scheme for this two-stage process is given in Figure 7.
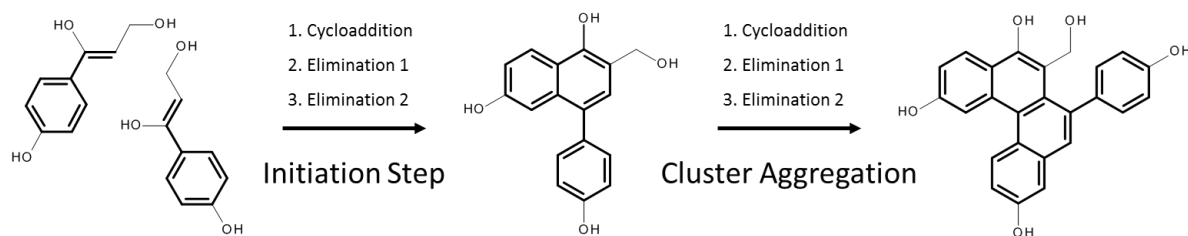

Figure 7. The proposed two-stage mechanism for char formation.

The initiation step begins with a Diels-Alder cycloaddition that concatenates two molecules of the β-O-4 derived model compound, forming a three-ringed intermediate complex. This is followed by one of two eliminations reactions which are dependent upon the isomerism of the

diene. Similarly, the nature of the second elimination reaction is dependent upon the dienophile isomerism. The cluster aggregation step, in which the initiation products now act as the diene, proceeds through the same set of potential reactions as the initiation step, however the first elimination reaction is now controlled by the structure of the cluster and its substituent groups.

3.5. Further applications of the char formation mechanism

Char is pervasive product formed during varying lignin pyrolysis processes. It has been shown that catalytic pyrolysis of lignin with zeolites is inhibited through catalyst deactivation by char formation. [67,68] Exploring potential reaction conditions that impede the progress of the cluster reaction mechanisms presented herein may indicate measures to reduce coke formation on catalysts. Furthermore, understanding the role that the Brønsted and Lewis acid sites within a zeolite framework may play on the proposed reaction mechanisms could identify ways to minimise char formation.

Both alkali metals and alkaline earth metals have been shown to influence the yields of char formed during lignocellulosic biomass pyrolysis. [69,70] Modelling the influence of alkali and alkaline earth ions on the mechanisms proposed here may help to clarify the specific role that metals play in coke formation and identify options to influence char formation.

It is well reported that cellulose and hemicellulose form pyrolysis char in the absence of lignin. [71–73] These chars are also shown to be formed of condensed aromatic structures and so may share similarities in their formation mechanisms to those presented here for lignin, particularly regarding the elimination reactions.

4. Conclusions

We have shown that char may be formed via a two-stage process that consists of an initiation stage and a subsequent cluster aggregation stage. A total of sixteen pathways were investigates for the initiation step, all of which start with a Diels-Alder cycloaddition. This ring-forming reaction is followed by second elementary reaction that is either a dehydrogenation reaction, or a methanol evolution reaction. The third elementary reaction of the initiation step is either a dehydration reaction or a Grob fragmentation reaction that yields formaldehyde in addition to water. All sixteen pathways lead to the formation of an oxygenated derivative of either 1-phenylnaphthalene or 2-phenylnaphthalene. The energy barriers of each step are commensurate

with those reported for other biomass pyrolysis reactions and all the generated secondary products are reported within the experimental lignin pyrolysis literature.

The mechanisms presented herein can be used as a basis for numerous further studies to better understand the role that catalytic species and materials play in lignin char evolution. Additionally, this work may also provide insights into potential routes for the formation of char from cellulosic biomass and their thermal degradation products.

Author Information

The manuscript was written through contributions from all authors. XZ contributed on conceptualization, data curation, formal analysis, funding acquisition, investigation, project administration, resources, software, supervision, visualization, and reviewing/editing the draft; AS contributed on data curation, formal analysis, investigation, methodology, and writing the original draft; SJ contributed on the investigation; JF contributed on the NMR testing; LL contributed on experimental validation, and reviewing/editing the draft; RB contributed on reviewing and editing the draft. All authors have given approval to the final version of the manuscript.

Competing interest statement

The authors would like to state that there is no competing interests.

Acknowledgements

References

1.   Wang, S., Dai, G., Yang, H. & Luo, Z. Lignocellulosic biomass pyrolysis mechanism: A state-of-the-art review. *Prog. Energy Combust. Sci.* **62**, 33–86 (2017).

2.   Collard, F. X. & Blin, J. A review on pyrolysis of biomass constituents: Mechanisms and

composition of the products obtained from the conversion of cellulose, hemicelluloses and lignin. *Renew. Sustain. Energy Rev.* **38**, 594–608 (2014).

3.   Bhutto, A. W. *et al.* Progress in the production of biomass-to-liquid biofuels to decarbonize the transport sector – prospects and challenges. *RSC Adv.* **6**, 32140–32170 (2016).

4.   Brewer, C. E., Schmidt-Rohr, K., Satrio, J. A. & Brown, R. C. Characterization of biochar from fast pyrolysis and gasification systems. *Environ. Prog. Sustain. Energy* **28**, 386–396 (2009).

5.   Le Brech, Y. *et al.* Characterization of biomass char formation investigated by advanced solid state NMR. *Carbon N. Y.* **108**, 165–177 (2016).

6.   Sharma, R. K. *et al.* Characterization of chars from pyrolysis of lignin. *Fuel* **83**, 1469–1482 (2004).

7.   Hu, Q. *et al.* Study on the physicochemical structure and gasification reactivity of chars from pyrolysis of biomass pellets under different heating rates. *Fuel* **314**, (2022).

8.   Qi, J., Fan, C., Wu, H. & Li, S. Structure evolution of lignite char in step pyrolysis and its combustion reactivity. *Fuel* **315**, (2022).

9.   Chen, Y. *et al.* Evolution of char structure during the pyrolysis of biomass pellet: Further understanding on the effects of chars two phases. *Fuel* **312**, (2022).

10.   Zheng, Q. *et al.* Insight into the fast pyrolysis of lignin: Unraveling the role of volatile evolving and char structural evolution. *Chem. Eng. J.* **437**, (2022).

11.   Hosoya, T., Kawamoto, H. & Saka, S. Pyrolysis gasification reactivities of primary tar and char fractions from cellulose and lignin as studied with a closed ampoule reactor. *J. Anal. Appl. Pyrolysis* **83**, 71–77 (2008).

12.   Sarve, D. T., Dutta, R., Rastogi, A. & Ekhe, J. D. Valorization of industrial waste lignin via pyrolysis in the presence of additives: Formation, characterization, and application of

fuel valued bio-oil and activated char. *J. Indian Chem. Soc.* **99**, (2022).

13.   Demirbas, A. Production and characterization of bio-chars from biomass via pyrolysis. *Energy Sources, Part A Recover. Util. Environ. Eff.* **28**, 413–422 (2006).

14.   Yang, H. *et al.* In-Depth Investigation of Biomass Pyrolysis Based on Three Major Components:‰ Hemicellulose, Cellulose and Lignin. *Energy Fuels* **20**, 388–393 (2006).

15.   Qu, T., Guo, W., Shen, L., Xiao, J. & Zhao, K. Experimental study of biomass pyrolysis based on three major components: Hemicellulose, cellulose, and lignin. *Ind. Eng. Chem. Res.* **50**, 10424–10433 (2011).

16.   Chakar, F. S. & Ragauskas, A. J. Review of current and future softwood kraft lignin process chemistry. *Ind. Crops Prod.* **20**, 131–141 (2004).

17.   Jarvis, M. W. *et al.* Direct detection of products from the pyrolysis of 2-phenethyl phenyl ether. *J. Phys. Chem. A* **115**, 428–438 (2011).

18.   Choi, Y. S. *et al.* Pyrolysis reaction networks for lignin model compounds: unraveling thermal deconstruction of β-O-4 and α-O-4 compounds. *Green Chem.* **18**, 1762–1773 (2016).

19.   Drage, T., Vane, C. & Abbott, G. The closed system pyrolysis of dimeric lignin moder compounds. *Org. Geochem.* **33**, 1523–1531 (2002).

20.   Britt, P. F., Kidder, M. K. & Buchanan, I. C. Oxygen substituent effects in the pyrolysis of phenethyl phenyl ethers. *Energy and Fuels* **21**, 3102–3108 (2007).

21.   Huang, X., Liu, C., Huang, J. & Li, H. Theory studies on pyrolysis mechanism of phenethyl phenyl ether. *Comput. Theor. Chem.* **976**, 51–59 (2011).

22.   Huang, J., Liu, C., Wu, D., Tong, H. & Ren, L. Density functional theory studies on pyrolysis mechanism of β-O-4 type lignin dimer model compound. *J. Anal. Appl. Pyrolysis* **109**, 98–108 (2014).

23.   Klein, M. T. & Vlrk, P. S. Model Pathways in Lignin Thermolysis. 1. Phenethyl Phenyl Ether. *Ind. Eng. Chem. Fundam.* **22**, 35–45 (1983).

24.   Chen, L. *et al.* Pyrolysis mechanism of β-O-4 type lignin model dimer. *J. Anal. Appl. Pyrolysis* **115**, 103–111 (2015).

25.   Jiang, W., Wu, S., Lucia, L. A. & Chu, J. A comparison of the pyrolysis behavior of selected B-O-4 type lignin model compounds. *J. Anal. Appl. Pyrolysis* **125**, 185–192 (2017).

26.   Elder, T. & Beste, A. Density functional theory study of the concerted pyrolysis mechanism for lignin models. *Energy and Fuels* **28**, 5229–5235 (2014).

27.   Zhao, Y., Schultz, N. E. & Truhlar, D. G. Design of density functionals by combining the method of constraint satisfaction with parametrization for thermochemistry, thermochemical kinetics, and noncovalent interactions. *J. Chem. Theory Comput.* **2**, 364–382 (2006).

28.   Elder, T. Bond dissociation enthalpies of a pinoresinol lignin model compound. *Energy and Fuels* **28**, 1175–1182 (2014).

29.   Younker, J. M., Beste, A. & Buchanan, A. C. Computational study of bond dissociation enthalpies for substituted β-O-4 lignin model compounds. *ChemPhysChem* **12**, 3556–3565 (2011).

30.   Wang, M., Liu, C., Xu, X. & Li, Q. Theoretical study of the pyrolysis of vanillin as a model of secondary lignin pyrolysis. *Chem. Phys. Lett.* **654**, 41–45 (2016).

31.   Zhao, Y. & Truhlar, D. G. The M06 suite of density functionals for main group thermochemistry, thermochemical kinetics, noncovalent interactions, excited states, and transition elements: Two new functionals and systematic testing of four M06-class functionals and 12 other function. *Theor. Chem. Acc.* **120**, 215–241 (2008).

32.   Goerigk, L. *et al.* A Look at the Density Functional Theory Zoo with the Advanced GMTKN55 Database for General Main Group Thermochemistry, Kinetics and

Noncovalent Interactions. *Phys. Chem. Chem. Phys.* **19**, 32184–32215 (2017).

33. Mardirossian, N. & Head-Gordon, M. ωb97X-V: A 10-parameter, range-separated hybrid, generalized gradient approximation density functional with nonlocal correlation, designed by a survival-of-the-fittest strategy. *Phys. Chem. Chem. Phys.* **16**, 9904–9924 (2014).

34. Karton, A. & Goerigk, L. Accurate reaction barrier heights of pericyclic reactions : Surprisingly large deviations for the CBS-QB3 composite method and their consequences in DFT benchmark studies. *J. Comput. Chem.* **36**, 622–632 (2015).

35. Zhao, Y. & Truhlar, D. G. Design of density functionals that are broadly accurate for thermochemistry, thermochemical kinetics, and nonbonded interactions. *J. Phys. Chem. A* **109**, 5656–5667 (2005).

36. Stephens, P. J., Devlin, F. J., Chabalowski, C. F. & Frisch, M. J. Ab Initio Calculation of Vibrational Absorption and Circular Dichroism Spectra Using Density Functional Force Fields. *J. Phys. Chem.* **98**, 11623–11627 (1994).

37. Grimme, S., Antony, J., Ehrlich, S. & Krieg, H. A consistent and accurate ab initio parametrization of density functional dispersion correction (DFT-D) for the 94 elements H-Pu. *J. Chem. Phys.* **132**, (2010).

38. Grimme, S., Ehrlich, S. & Goerigk, L. Effect of the damping function in dispersion corrected density functional theory. *J. Comput. Chem.* **32**, 1456–1465 (2011).

39. Baboul, A. G., Curtiss, L. A., Redfern, P. C. & Raghavachari, K. Gaussian-3 theory using density functional geometries and zero-point energies. *J. Chem. Phys.* **110**, 7650–7657 (1999).

40. Weigend, F. & Ahlrichs, R. Balanced basis sets of split valence, triple zeta valence and quadruple zeta valence quality for H to Rn: Design and assessment of accuracy. *Phys. Chem. Chem. Phys.* **7**, 3297 (2005).

41. Frisch, M. J. *et al.* Gaussian 16, revision A. 03. *Gaussian Inc., Wallingford CT* (2016).

42. Lang, L., Zhao, S., Jiang, J., Yang, W. & Yin, X. Importance of hydrogen for low-temperature detemplation of high-silica MFI zeolite crystals. *Microporous Mesoporous Mater.* **235**, 143–150 (2016).

43. Jiang, J. F. *et al.* Partial Oxidation of Filter Cake Particles from Biomass Gasification Process in the Simulated Product Gas Environment. *Energy and Fuels* **32**, 1703–1710 (2018).

44. Akiyama, T., Sugimoto, T., Matsumoto, Y. & Meshitsuka, G. Erythro/threo ratio of β-O-4 structures as an important structural characteristic of lignin. I: Improvement of ozonation method for the quantitative analysis of lignin side-chain structure. *J. Wood Sci.* **48**, 210–215 (2002).

45. Akiyama, T. *et al.* Erythro/threo ratio of β-O-4-structures as an important structural characteristic of lignin. Part 4: Variation in the erythro/threo ratio in softwood and hardwood lignins and its relation to syringyl/guaiacyl ratio. *Holzforschung* **59**, 276–281 (2005).

46. Khuong, K. S., Jones, W. H., Pryor, W. A. & Houk, K. N. The Mechanism of the Self-Initiated Thermal Polymerization of Styrene. Theoretical Solution of a Classic Problem. (2004). doi:10.1021/ja0448667

47. Mayo, F. R. Chain Transfer in the Polymerization of Styrene. VIII. Chain Transfer with Bromobenzene and Mechanism of Thermal Initiation. *J. Am. Chem. Soc.* **75**, 6133–6141 (1953).

48. Ellis, R. J. & Frey, H. M. The thermal unimolecular isomerisation of bicyclo[3,1,0]hex-2-ene and decomposition of cyclohexa-1,4-diene. *J. Chem. Soc. A Inorganic, Phys. Theor.* 553–556 (1966). doi:10.1039/J19660000553

49. Benson, S. W. & Shaw, R. Kinetics and mechanism of the pyrolysis of 1,4-cyclohexadiene. *Trans. Faraday Soc.* **63**, 985–992 (1967).

50. Moon, S., Kwon, Y. & Choo, J. Vibrational spectra and conformations of 1,4-cyclohexadiene and its oxygen analogues: Ab initio and density functional calculations. *J.*

Mol. Struct. **470**, 265–275 (1998).

51.   Uchiyama, M., Tomioka, T. & Amano, A. Thermal decomposition of cyclohexene. *J. Phys. Chem.* **68**, 1878–1881 (1964).

52.   Smith, S. R. & Gordon, A. S. A STUDY OF THE PYROLYSIS OF CYCLOHEXENE [1]. *J. Phys. Chem.* **65**, 1124–1128 (1961).

53.   Ipatieff, V. N., Czajkowski, G. J. & Pines, H. Study in Terpene Series. XI. [1] The Dehydroxymethylation of Bicyclic Primary Terpenic Alcohols by Hydrogenolysis in the Presence of Nickel Catalysts [2]. *J. Am. Chem. Soc.* **73**, 4098–4101 (1951).

54.   Pines, H., Rodenberg, H. G. & Ipatieff, V. N. Dehydroxymethylation of Primary Alcohols. *J. Am. Chem. Soc.* **76**, 771–772 (1954).

55.   Modak, A., Naveen, T. & Maiti, D. An efficient dehydroxymethylation reaction by a palladium catalyst. *Chem. Commun.* **49**, 252–254 (2013).

56.   Allan, G. G. & Mattila, T. *High energy degradation, in lignins – Occurrence, Formation Structure and Reactions*. (Wiley-Interscience, 1971).

57.   Klein, M. T. & Virk, P. S. *Model pathways in lignin thermolysis. ENERGY LABORATORY REPORT NO. MIT-EL 81-005* (1981).

58.   Khachatryan, L., Xu, M. X., Wu, A. J., Pechagin, M. & Asatryan, R. Radicals and molecular products from the gas-phase pyrolysis of lignin model compounds. Cinnamyl alcohol. *J. Anal. Appl. Pyrolysis* **121**, 75–83 (2016).

59.   Xu, M. X., Khachatryan, L., Baev, A. & Asatryan, R. Radicals from the gas-phase pyrolysis of a lignin model compound: p-coumaryl alcohol. *RSC Adv.* **6**, 62399–62405 (2016).

60.   Kuroda, K. Analytical pyrolysis products derived from cinnamyl alcohol-end groups in lignins. *J. Anal. Appl. Pyrolysis* **53**, 123–134 (2000).

61.   Nimlos, M. R., Blanksby, S. J., Qian, X., Himmel, M. E. & Johnson, D. K. Mechanisms of

glycerol dehydration. *J. Phys. Chem. A* **110**, 6145–6156 (2006).

62.   Paine, J. B., Pithawalla, Y. B., Naworal, J. D. & Thomas, C. E. Carbohydrate pyrolysis mechanisms from isotopic labeling. Part 1: The pyrolysis of glycerin: Discovery of competing fragmentation mechanisms affording acetaldehyde and formaldehyde and the implications for carbohydrate pyrolysis. *J. Anal. Appl. Pyrolysis* **80**, 297–311 (2007).

63.   Jakab, E., Faix, O., Till, F. & Székely, T. Thermogravimetry/mass spectrometry study of six lignins within the scope of an international round robin test. *J. Anal. Appl. Pyrolysis* **35**, 167–179 (1995).

64.   Sivaramakrishnan, R. *et al.* Rate constants for the thermal decomposition of ethanol and its bimolecular reactions with OH and D: Reflected shock tube and theoretical studies. *J. Phys. Chem. A* **114**, 9425–9439 (2010).

65.   Accurate Quantification of Aromaticity and Nonprotonated Aromatic Carbon Fraction in Natural Organic Matter by 13 C Solid-State Nuclear Magnetic Resonance. (2004). doi:10.1021/es034770x

66.   Solum, M. S., Pugmire, R. J. & Grant, D. M. *Solid-State NMR of Argonne Premium Coals*. *Energy & Fuels* **3**, (1989).

67.   Zhang, H., Wang, Y., Shao, S. & Xiao, R. Catalytic conversion of lignin pyrolysis model compound- guaiacol and its kinetic model including coke formation. *Sci. Rep.* **6**, 1–10 (2016).

68.   Lazaridis, P. A., Fotopoulos, A. P., Karakoulia, S. A. & Triantafyllidis, K. S. Catalytic fast pyrolysis of kraft lignin with conventional, mesoporous and nanosized ZSM-5 zeolite for the production of alkyl-phenols and aromatics. *Front. Chem.* **6**, (2018).

69.   Eom, I. Y. *et al.* Effect of essential inorganic metals on primary thermal degradation of lignocellulosic biomass. *Bioresour. Technol.* **104**, 687–694 (2012).

70.   Jakab, E., Faix, O., Till, F. & Székely, T. The effect of cations on the thermal decomposition of lignins. *J. Anal. Appl. Pyrolysis* **25**, 185–194 (1993).

71.   Yang, H. *et al.* Cellulose Pyrolysis Mechanism Based on Functional Group Evolutions by Two-Dimensional Perturbation Correlation Infrared Spectroscopy. *Energy and Fuels* **34**, 3412–3421 (2020).

72.   Zhang, C. *et al.* Pyrolysis of cellulose: Evolution of functionalities and structure of bio-char versus temperature. *Renew. Sustain. Energy Rev.* **135**, 110416 (2021).

73.   Ma, Z. *et al.* In-depth comparison of the physicochemical characteristics of bio-char derived from biomass pseudo components: Hemicellulose, cellulose, and lignin. *J. Anal. Appl. Pyrolysis* **140**, 195–204 (2019).